CALCULATION OF SUSPENDING FORCE FOR NEW BEARINGLESS SWITCHED RELUCTANCE MOTOR

Huijun Wang, Dong-Hee Lee, Jin-Woo Ahn
Dept. of Electrical and Mechatronics Engineering, Kyungsung University, Busan, 608-736, Korea
huijun024@gmail.com, leedh@ks.ac.kr, jwahn@ks.ac.kr

ABSTRACT

In order to decouple the rotational torque and suspending radial force from stator winding, a novel bearingless switched reluctance motor (BLSRM) with hybrid stator poles structure is proposed in this paper. The proposed BLSRM has wide stator poles in rectangular axis. And other stator poles generate torque. So, it can be controlled the air-gap more easily with decoupled suspending radial force. The simple structure can reduce the number of power devices. A prototype design is analyzed by the finite element method (FEM) and mathematic model to evaluate the performances. The validity of structure and mathematic model is verified by simulation results.

INTRODUCTION

In modern industrial field, such as machine tool, molecular pump, centrifuge, compressor and aerospace need high speed and ultra-high speed machine. The switched reluctance motor (SRM) is a double salient, single excited motor. The stator consists of simple concentric windings. And there are no windings or permanent magnets on the rotor. Therefore, SRM is suitable for high speed machine. However, the mechanical bearing can cause friction, thermal problem and mechanical failure in a high speed range. This not only leads to lower efficiency of machine and reduction in service life of bearings, but also increases burden of maintenance for machine and bearings.

In order to solve above problems, recently various bearingless switched reluctance motors (BLSRM) have been researched [1]-[3]. In this paper, a novel BLSRM structure with hybrid stator poles is proposed. And one 8/10 BLSRM prototype is designed and manufactured. In order to carry out real-time control of BLSRM, calculation model for suspending force is developed. In this model, significant fringing flux between the stator and rotor is considered. And eccentric errors in x and y directions are taken into account. The validity of structure and calculation model is verified by finite element analysis (FEA) and simulation results.

STRUCTURE AND PRINCIPLES

Conventional BLSRM

Fig. 1 shows structure and operating principle of the conventional BLSRM. For conventional BLSRM, it should be noted that the 4-pole flux produced by the currents of motor torque winding, is essential as the bias magnetic flux for suspension force generation. This also means radial force can not be produced if no currents flow through torque winding.

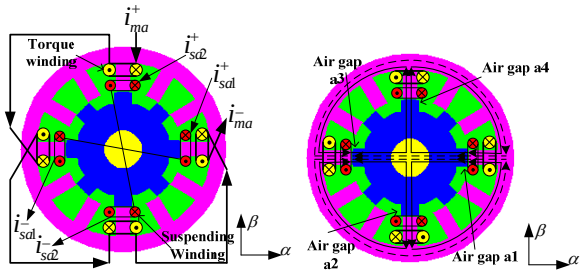

(a) Basic structure (b) operating principle

FIGURE1: Conventional BLSRM

Curves of inductance, radial force and torque can be obtained through FEM and shown in Fig.2. From this figure, we can find that from θ_1 to θ_3 is the torque region. From θ_2 to θ_4 is radial force region. Overlap region between generating rotational torque and radial force is from θ_2 to θ_3. Ideally it is best for motor to operate in this overlap region, in which enough torque and radial force can be generated at the same time. However, because of inherent principle of torque and radial force in SRM, this overlap region is very narrow. And operating point has to be selected in compromise between torque and radial force when using conventional structure. Accordingly, regions of torque production and radial force can not be fully utilized. In order to get an enough radial force, current has to be increased and dwell angle should be moved toward aligned position. This will result into high copper loss and large negative torque. So, efficiency is reduced, thermal load is increased and speed is limited.

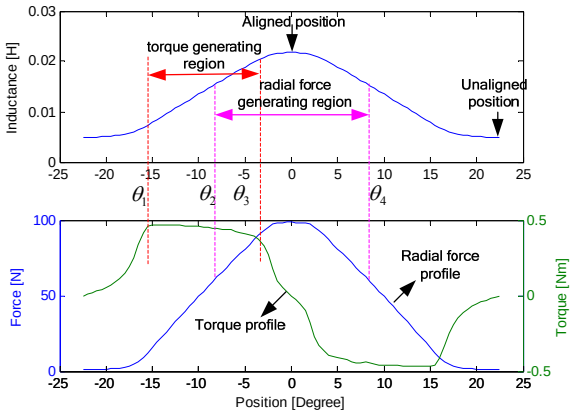

FIGURE2: Inductance, torque and radial force profiles in conventional BLSRM

Proposed BLSRM

Fig. 3(a) shows structures of proposed BLSRM. In Fig. 3(a), different from conventional structure, two types of stator poles are included on the stator. One is torque pole such as A1, A2, B1 and B2, which mainly produce rotational torque. The other is radial force pole such as P_{x1}, P_{x2}, P_{x3} and P_{x4}, which mainly generate radial force to suspend rotor and shaft. At the same time pole arc of radial force pole is one pole pitch of rotor for producing continuous radial force. Windings on the pole A1 and pole A2 are connected in series to construct torque winding A, and windings on the pole B1 and pole B2 are connected in series to construct torque winding B. windings on poles P_{x1}, P_{x2}, P_{x3} and P_{x4} are independently controlled to construct four radial force windings P1, P2, P3 and P4 in x and y directions.

Fig. 3(b) shows control principle of suspending force. From this figure, when rotor has eccentric displacement in positive y-direction, only current i_2 will be turned on and other radial force winding P_{x1}, P_{x2} and P_{x3} are turned off. Accordingly radial force in negative y-direction is generated. Current i_2 can be regulated until rotor is in balanced position. Using same method, if rotor has eccentric displacement in positive x-direction at the same time, only winding P_{x3} needs to be turned on and current i_3 is regulated to make rotor return to its zero eccentric position.

CALCULATION MODEL OF SUSPENDING FORCE

The following assumptions are considered for simple analysis:

1. Magnetic saturation can be neglected.
2. Leakage flux is ignored.
3. Axial eccentricity is small compared with length of air-gap.

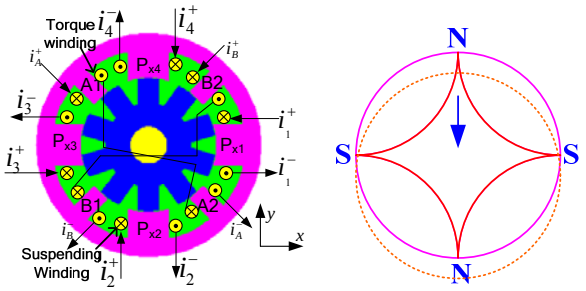

(a) Proposed BLSRM (b) Suspending control principle

FIGURE3: Structure and control principle of proposed BLSRM

Permeance Analysis

In proposed structure, pole-arc of rotor is β_r, and stator pole-arc for suspending force is one pole pitch of rotor τ_r. At the same time β_0 is defined as $1/2(\tau_r - \beta_r)$. When relation between β_0 and the sum of rotor angle θ and displacement β in the y direction is different, model of magnetic conductance is also different. In Fig. 4 (a) and (b) magnetic field distribution of two cases with $r\theta+\beta \le \beta_0$ and $\beta_0 \le r\theta+\beta \le (\beta_0+0.5\beta_r)$ are shown.

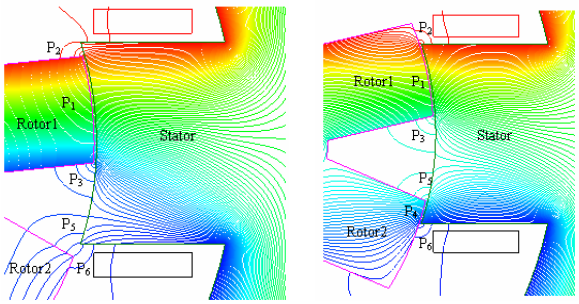

(a) $r\theta+\beta \le \beta_0$ (b) $\beta_0 \le r\theta+\beta \le (\beta_0+0.5\beta_r)$

FIGURE4: Magnetic field distribution of air-gap

According to Fig. 4, simplified equivalent magnetic circuits for two cases are shown in Fig. 5.

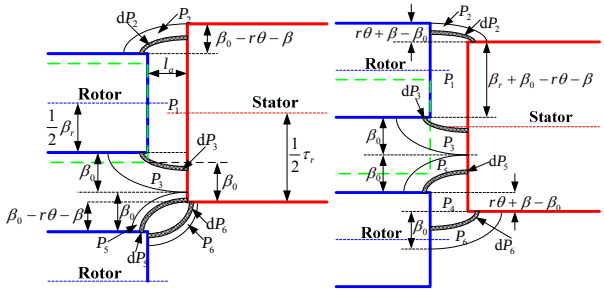

(a) $r\theta+\beta \le \beta_0$ (b) $\beta_0 \le r\theta+\beta \le (\beta_0+0.5\beta_r)$

FIGURE5: Simplified equivalent magnetic circuit of air-gap

case1: rθ+β≤β₀

In Fig. 5(a), magnetic conductance can be divided into five parts. Overlap part P_1 between stator and rotor can be simplified as linear magnetic circuit. Other parts such as P_2, P_3, P_4 and P_5 can be considered as elliptical magnetic circuits. Therefore P_1 can be described as following equation [4]:

$$P_1 = \int_0^{\beta_r} \frac{\mu_0 l \mathrm{d}x}{l_0 - \alpha + \frac{\beta\theta}{2}} = \frac{\mu_0 l \beta_r}{l_0 - \alpha + \frac{\beta\theta}{2}} \tag{1}$$

in which, l is axial length of core, μ_0 is permeability, l_0 is length of air-gap without eccentricity and α is eccentric displacement in x-axis direction.

From Fig. 5(a), it can be seen that solvable ranges of P_2, P_3, P_5 and P_6 are [0, β_0-rθ-β], [0, β_0], [β_0-rθ-β, β_0] and [β_0-rθ-β, β_0]. So corresponding magnetic conductance of these parts can be expressed as following equations:

$$\begin{aligned} P_2 &= \int_0^{\beta_0 - r\theta - \beta} \frac{\mu_0 l(al_a + 2x)\mathrm{d}x}{(2l_a + \pi x)(al_a + x)} \\ &= \frac{\mu_0 l}{a\pi - 2}\left[a \ln \frac{al_a - r\theta - \beta + \beta_0}{al_a} + \frac{a\pi - 4}{\pi} \ln \frac{2l_a + \pi(-r\theta - \beta + \beta_0)}{2l_a} \right] \end{aligned} \tag{2}$$

$$\begin{aligned} P_3 &= \int_0^{\beta_0} \frac{\mu_0 l(al_a + 2x)\mathrm{d}x}{(2l_a + \pi x)(al_a + x)} \\ &= \frac{\mu_0 l}{a\pi - 2}\left[a \ln \frac{al_a + \beta_0}{al_a} + \frac{a\pi - 4}{\pi} \ln \frac{2l_a + \pi\beta_0}{2l_a} \right] \end{aligned} \tag{3}$$

$$\begin{aligned} P_5 = P_6 &= \int_{\beta_0 - r\theta - \beta}^{\beta_0} \frac{\mu_0 l(al_a + 2x)\mathrm{d}x}{(2l_a + \pi x)(al_a + x)} \\ &= \frac{\mu_0 l}{a\pi - 2}\left[\begin{array}{l} a \ln \frac{al_a + \beta_0}{al_a} + \frac{a\pi - 4}{\pi} \ln \frac{2l_a + \pi\beta_0}{2l_a} \\ - a \ln \frac{al_a - r\theta - \beta + \beta_0}{al_a} - \\ \frac{a\pi - 4}{\pi} \ln \frac{2l_a + \pi(-r\theta - \beta + \beta_0)}{2l_a} \end{array} \right] \end{aligned} \tag{4}$$

in which a is coefficient acquired through FEM analysis, l_a is described as (5)[5]:

$$l_a = l_0 - \alpha + \frac{\beta\theta}{2} \tag{5}$$

So all magnetic conductance of air-gap P_{x1} is shown in (6).

case2: β₀≤rθ+β≤ (β₀+0.5βᵣ)

From Fig. 5(b), magnetic conductance can be divided into six parts. Overlap parts between stator and rotor P_1 and P_4 can be simplified as linear magnetic circuits. Other parts can be considered as elliptical magnetic circuits. Solvable ranges from P_1 to P_6 are [0, β_r+β_0-rθ-β], [0, rθ+β-β_0], [0, β_0], [0, rθ+β-β_0], [0, β_0] and [0, β_0], respectively. Therefore P_1 and P_4 can be described as (7) to (10).

$$\begin{aligned} P_{x1} &= P_1 + P_2 + P_3 + 2P_5 \\ &= \frac{\mu_0 l \beta_r}{l_0 - \alpha + \frac{\beta\theta}{2}} + 3\frac{\mu_0 l}{a\pi - 2}\left[a \ln \frac{al_a + \beta_0}{al_a} + \frac{a\pi - 4}{\pi} \ln \frac{2l_a + \pi\beta_0}{2l_a} \right] \\ &\quad - \frac{\mu_0 l}{a\pi - 2}\left[a \ln \frac{al_a - r\theta - \beta + \beta_0}{al_a} + \frac{a\pi - 4}{\pi} \ln \frac{2l_a + \pi(-r\theta - \beta + \beta_0)}{2l_a} \right] \end{aligned} \tag{6}$$

$$P_1 = \int_0^{\beta_r + \beta_0 - r\theta - \beta} \frac{\mu_0 l \mathrm{d}x}{l_0 - \alpha + \frac{\beta\theta}{2}} = \frac{\mu_0 l(\beta_r + \beta_0 - r\theta - \beta)}{l_0 - \alpha + \frac{\beta\theta}{2}} \tag{7}$$

$$\begin{aligned} P_2 &= \int_0^{r\theta + \beta - \beta_0} \frac{\mu_0 l(al_a + 2x)\mathrm{d}x}{(2l_a + \pi x)(al_a + x)} \\ &= \frac{\mu_0 l}{a\pi - 2}\left[a \ln \frac{al_a + r\theta + \beta - \beta_0}{al_a} + \frac{a\pi - 4}{\pi} \ln \frac{2l_a + \pi(r\theta + \beta - \beta_0)}{2l_a} \right] \end{aligned} \tag{8}$$

$$P_4 = \int_0^{r\theta + \beta - \beta_0} \frac{\mu_0 l \mathrm{d}x}{l_0 - \alpha + \frac{\beta\theta}{2}} = \frac{\mu_0 l(r\theta + \beta - \beta_0)}{l_0 - \alpha + \frac{\beta\theta}{2}} \tag{9}$$

$$\begin{aligned} P_3 = P_5 = P_6 &= \int_0^{\beta_0} \frac{\mu_0 l(al_a + 2x)\mathrm{d}x}{(2l_a + \pi x)(al_a + x)} \\ &= \frac{\mu_0 l}{a\pi - 2}\left[a \ln \frac{al_a + \beta_0}{al_a} + \frac{a\pi - 4}{\pi} \ln \frac{2l_a + \pi\beta_0}{2l_a} \right] \end{aligned} \tag{10}$$

So all magnetic conductance of air-gap P_{x1} is equal to:

$$\begin{aligned} P_{x1} &= P_1 + P_2 + P_3 + P_4 + P_5 + P_6 \\ &= \frac{\mu_0 l \beta_r}{l_0 - \alpha + \frac{\beta\theta}{2}} + 3\frac{\mu_0 l}{a\pi - 2}\left[a \ln \frac{al_a + \beta_0}{al_a} + \frac{a\pi - 4}{\pi} \ln \frac{2l_a + \pi\beta_0}{2l_a} \right] \\ &\quad + \frac{\mu_0 l}{a\pi - 2}\left[a \ln \frac{al_a + r\theta + \beta - \beta_0}{al_a} + \frac{a\pi - 4}{\pi} \ln \frac{2l_a + \pi(r\theta + \beta - \beta_0)}{2l_a} \right] \end{aligned} \tag{11}$$

From symmetric structure of BLSRM, air-gap permeances of P_{x2}, P_{x3} and P_{x4} can be calculated using same method.

Suspending Force Calculation

Taking P_{X1} suspending winding as the example, radial

forces in x direction F_α and in y direction F_β are deduced as following method.

As we know permeability of air-gap is constant, permeances P_{x1}, P_{x2}, P_{x3} and P_{x4} are only related to dimensions of motor. And the stored electromagnetic energy can be expressed as following equation:

$$W_a = \frac{1}{2}Li^2 = \frac{1}{2}P(Ni)^2 \tag{12}$$

in which, i is current, P is permeance of air-gap, N is winding turn.

Therefore energy at Px1 is

$$W_{x1} = \frac{1}{2}P_{x1}(Ni)^2 \tag{13}$$

Further, radial forces F_α, F_β can be derived from the derivatives of energy with respect to displacement α, β and angle of rotor.

$$F_\alpha = \frac{\partial W_{x1}}{\partial \alpha} = \frac{1}{2}\frac{\partial P_{x1}}{\partial \alpha}(Ni)^2 \tag{14}$$

$$F_\beta = \frac{\partial W_{x1}}{\partial \beta} = \frac{1}{2}\frac{\partial P_{x1}}{\partial \beta}(Ni)^2 \tag{15}$$

According to symmetric structure, only period [0, β_0+0.5β_r] is considered. At the same time, solution of radial force is also divided in two cases.

case1: rθ+β≤β_0

According to (6), (14) and (15), suspending forces in x and y directions can be obtained as following equations:

$$\frac{\partial P_{x1}}{\partial \alpha} = \frac{\mu_0 l\beta_r}{\left(l_0-\alpha+\frac{\beta\theta}{2}\right)^2} + 3\frac{\mu_0 l}{a\pi-2}\left\{\begin{array}{l}\dfrac{-a^2}{a\left(l_0-\alpha+\frac{\beta\theta}{2}\right)+\beta_0}+\dfrac{a}{l_0-\alpha+\frac{\beta\theta}{2}} \\ +\dfrac{a\pi-4}{\pi}\left[\dfrac{-2}{2\left(l_0-\alpha+\frac{\beta\theta}{2}\right)+\pi\beta_0}+\dfrac{1}{l_0-\alpha+\frac{\beta\theta}{2}}\right]\end{array}\right\} \tag{16}$$

$$-\frac{\mu_0 l}{a\pi-2}\left\{\begin{array}{l}\dfrac{-a^2}{a\left(l_0-\alpha+\frac{\beta\theta}{2}\right)-r\theta-\beta+\beta_0}+\dfrac{a}{l_0-\alpha+\frac{\beta\theta}{2}} \\ +\dfrac{a\pi-4}{\pi}\left[\dfrac{-2}{2\left(l_0-\alpha+\frac{\beta\theta}{2}\right)+\pi(\beta_0-\beta-r\theta)}+\dfrac{1}{l_0-\alpha+\frac{\beta\theta}{2}}\right]\end{array}\right\}$$

$$\frac{\partial P_{x1}}{\partial \beta} \approx \frac{-\mu_0 l\beta_r}{\left(l_0-\alpha+\frac{\beta\theta}{2}\right)^2}\frac{\theta}{2} \tag{17}$$

case2: β_0≤rθ+β≤ (β_0+0.5β_r)

According to equations (11), (14) and (15), suspending forces in x and y directions can be obtained as following equations:

$$\frac{\partial P_{x1}}{\partial \alpha} = \frac{\mu_0 l\beta_0}{\left(l_0-\alpha+\frac{\beta\theta}{2}\right)^2} + 3\frac{\mu_0 l}{a\pi-2}\left\{\begin{array}{l}\dfrac{-a^2}{a\left(l_0-\alpha+\frac{\beta\theta}{2}\right)+\beta_0}+\dfrac{a}{l_0-\alpha+\frac{\beta\theta}{2}} \\ +\dfrac{a\pi-4}{\pi}\left[\dfrac{-2}{2\left(l_0-\alpha+\frac{\beta\theta}{2}\right)+\pi\beta_0}+\dfrac{1}{l_0-\alpha+\frac{\beta\theta}{2}}\right]\end{array}\right\} \tag{18}$$

$$+\frac{\mu_0 l}{a\pi-2}\left\{\begin{array}{l}\dfrac{-a^2}{a\left(l_0-\alpha+\frac{\beta\theta}{2}\right)+r\theta+\beta-\beta_0}+\dfrac{a}{l_0-\alpha+\frac{\beta\theta}{2}} \\ +\dfrac{a\pi-4}{\pi}\left[\dfrac{-2}{2\left(l_0-\alpha+\frac{\beta\theta}{2}\right)+\pi(r\theta+\beta-\beta_0)}+\dfrac{1}{l_0-\alpha+\frac{\beta\theta}{2}}\right]\end{array}\right\}$$

$$\frac{\partial P_{x1}}{\partial \beta} \approx \frac{\mu_0 l}{\left(l_0-\alpha+\frac{\beta\theta}{2}\right)^2}\left[-\frac{\theta}{2}(2\beta_r+\beta_0-2r\theta-2\beta)\right] \tag{19}$$

FEA Comparison

Finite element method is applied to calculate suspending force. Figs. 6 and 7 show compared results between FEA and calculation model. From these two figures we can find that values obtained from calculation model coincide well with that of FEA results.

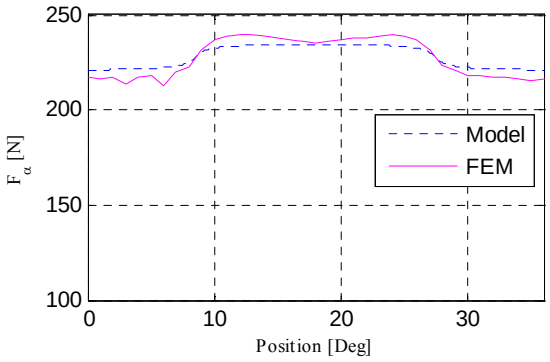

FIGURE6: Suspending force in the x direction

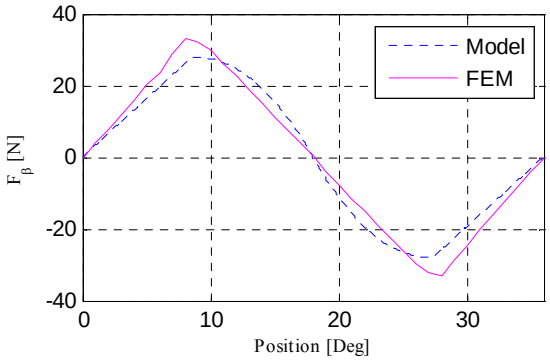

FIGURE7: Suspending force in the y direction

DESIGN OF NOVEL BLSRM

Based on above analysis, 8/10 prototype motor is designed and manufactured. Fig. 8 shows its stator and rotor. Detailed specifications of proposed BLSRM are shown in TABLE 1.

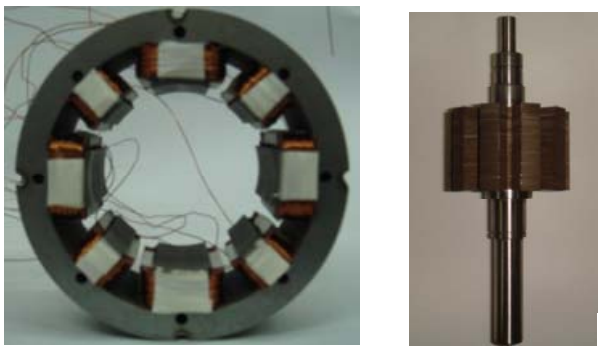

(a) Stator (b) Rotor

FIGURE8: Stator and rotor of proposed BLSRM

TABLE 1: Specifications of prototype BLSRM

Parameter	Value
Number of Stator Poles	8
Number of Rotor Poles	10
Pole arc of stator for torque [deg]	18
Pole arc of stator for radial force [deg]	36
Pole arc of rotor [deg]	18
Length of axial stack [mm]	40
Outer Diameter of Stator [mm]	112
Inner Diameter of Stator [mm]	62
Yoke Thickness of Stator [mm]	10
Length of Air Gap [mm]	0.3
Inner Diameter of Rotor [mm]	18
Yoke Thickness of Rotor [mm]	9.7

At the same time, according to (14) to (19), suspending forces profiles of stator pole P_{x1} can be obtained as shown in Fig. 9 and 10.

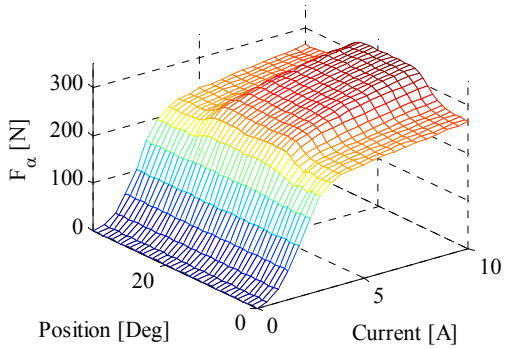

FIGURE9: Suspending force profile in x direction in P_{x1} of the proposed BLSRM

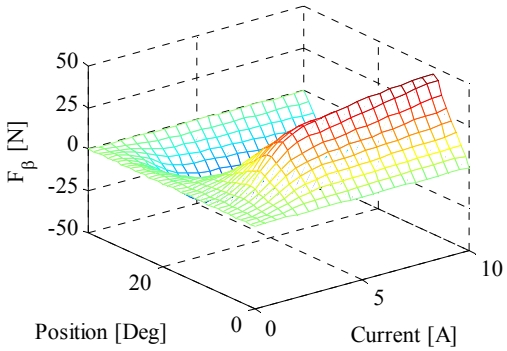

FIGURE10: Suspending force profile in y direction P_{x1} of the proposed BLSRM

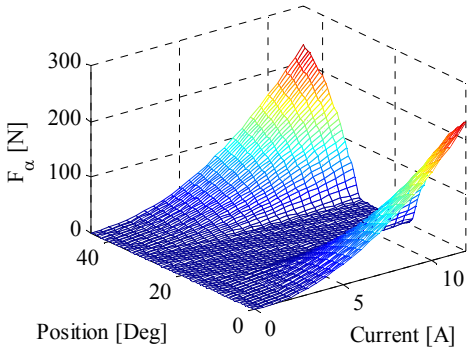

FIGURE11: Suspending force profile in x direction of conventional BLSRM

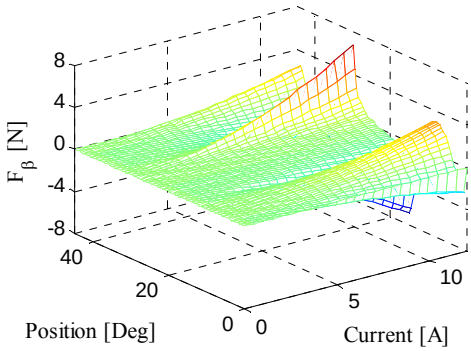

FIGURE12: Suspending force profile in y direction of conventional BLSRM

In order to explain the merits of proposed structure, conventional BLSRM is also analyzed as shown in Fig. 11 and 12. From Fig.9 to 12, radial force in proposed structure almost keeps constant with the variation of rotor position. However in the conventional structure, radial force varies noticeable with rotor position.

Therefore, for conventional BLSRM, conducting period has to be selected in compromise between torque and radial force. At the same time current has to be increased for generating enough suspending force. This causes complex control scheme and large torque ripple. However, for proposed BLSRM, much lower current and simpler control algorithm can be obtained due to good suspending force characteristic.

SIMULATION RESULTS

To guarantee a steady operation of BLSRM, the radial force should be controlled at all position. Fig. 13 shows control block diagram of the proposed system.

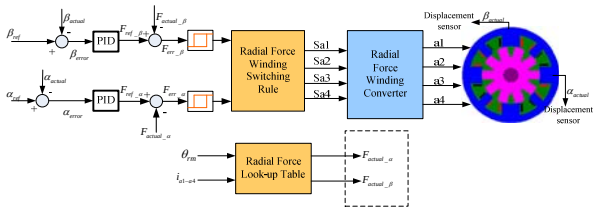

FIGURE13: Suspending force control block diagram of proposed BLSRM

From Fig. 13, air-gap displacement errors in two directions are input to PID controllers to generate radial force references. And through current and position, actual radial forces can be obtained by look-up tables. Then two radial force errors are input to two hystersis controllers, accordingly control signal can be generated when using some control rules.

In the simulation, suspending load in the y direction is 10N. Rotor speed is 1500rpm. Initial eccentric displacements in x and y directions are 60μm. Current is limited at 10A. Current ia_1 to ia_4 are suspending current i_1 to i_4, respectively. Figs. 14 to 18 show simulation results.

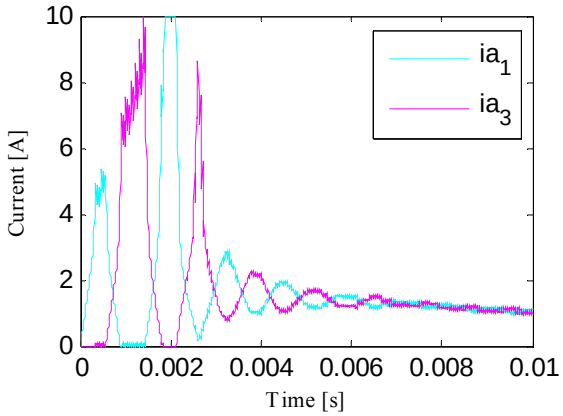

FIGURE14: Suspending currents ia_1 and ia_3

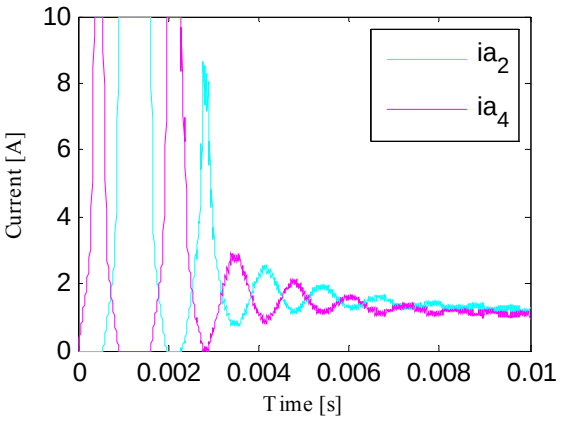

FIGURE15: Suspending currents ia_2 and ia_4

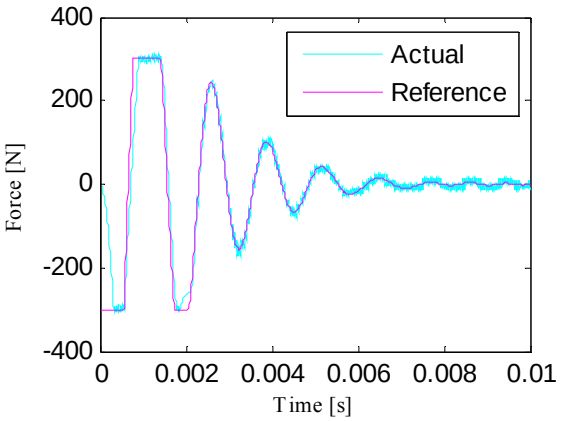

FIGURE16: Suspending force in x-direction

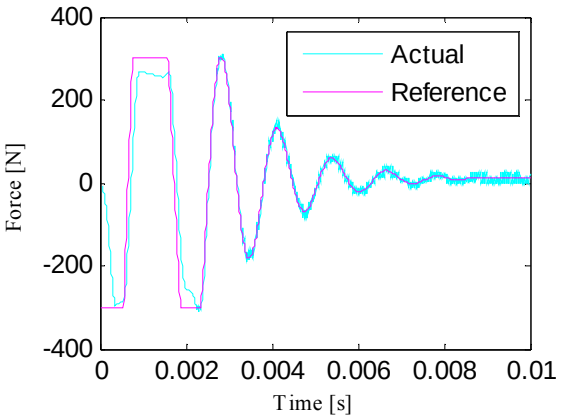

FIGURE17: Suspending force in y-direction

From simulation results, four suspending currents are independently regulated to control suspending force in x and y directions. Eccentric error of rotor can be

gradually reduced as shown in Fig. 18.

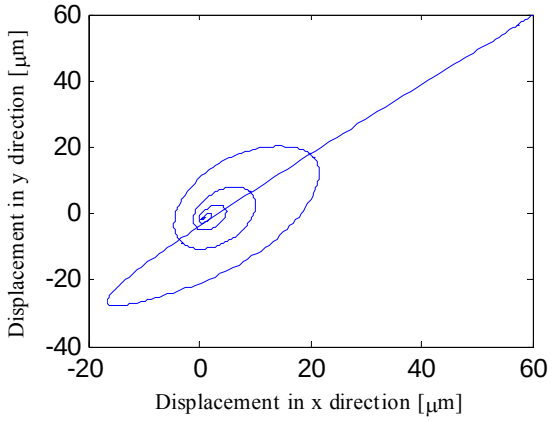

FIGURE18: Rotor locus

CONCLUSIONS

In this paper, a novel structure of BLSRM with hybrid stator poles is proposed. In order to implement real-time control of BLSRM, calculation model for suspending force is introduced. Compared with conventional BLSRM, proposed structure has many advantages such as lower thermal load, simpler control algorithm. The validity of mathematical model for suspending force is verified by FEM and simulation results.

ACKNOWLEDGMENT

This work has been supported by EIRC (I-2007-0-261-01), which is funded by MKE (Ministry of Knowledge & Economy) and ETEP (Electric Power Industry Technology Evaluation &Planning), Korea.

REFERENCE

1. M. Takemoto, A. Chiba, H. Akagi and T. Fukao, “Radial Force and Torque of a Bearingless Switched Reluctance Motor Operating in a Region of Magnetic Saturation” in Conf. Record IEEE-IAS Annual Meeting, 2002, pp. 35 - 42.
2. Li Chen, Wilfried Hofmann, “Analytically Computing Winding Currents to Generate Torque and Levitation Force of a New Bearingless Switched Reluctance Motor”, in Proc.12th EPE-PEMC, Aug, 2006, pp. 1058-1063.
3. Carlos R. Morrison. Bearingless Switched Reluctance Motor. U.S. Patent 6,727,618, 2004.
4. Shuang Ye. Research on Bearingless Switched Reluctance Motors, Master’s thesis, 2003.
5. Qiurong Wang. Analysis And Design of Bearingless Switched Reluctance Motor. Master’s thesis, 2007.